Control of the Morphology and Structural Development of Solution-Processed Functionalized Acenes for High-Performance Organic Transistors

By *Jung Ah Lim, Hwa Sung Lee, Wi Hyoung Lee,* and *Kilwon Cho**

Solution-processable functionalized acenes have received special attention as promising organic semiconductors in recent years because of their superior intermolecular interactions and solution-processability, and provide useful benchmarks for organic field-effect transistors (OFETs). Charge-carrier transport in organic semiconductor thin films is governed by their morphologies and molecular orientation, so self-assembly of these functionalized acenes during solution processing is an important challenge. This article discusses the charge-carrier transport characteristics of solution-processed functionalized acene transistors and, in particular, focuses on the fine control of the films' morphologies and structural evolution during film-deposition processes such as inkjet printing and post-deposition annealing. We discuss strategies for controlling morphologies and crystalline microstructure of soluble acenes with a view to fabricating high-performance OFETs.

1. Introduction

Following the discovery of field-effect charge-carrier conduction in small organic molecules and conjugated polymers, organic field-effect transistors (OFETs) containing these organic semiconductors as active layers have been seen as a potential alternative to mainstream thin-film transistors based on inorganic materials.[1–3] One of their particular attractions is that all the layers of an OFET can easily be deposited at room temperature with solution-processing or direct-write printing, which means that with their use low-cost, large-area electronic devices can be realized on flexible substrates.[4,5] However, in spite of considerable progress during recent years, the electrical properties of OFETs fabricated with solution processing remain very much inferior to those of their inorganic counterparts.

Charge-carrier transport in an OFET is strongly related to the morphology and crystalline microstructure of the organic semiconductor film. It is known that charge-carrier transport is limited by hopping between the molecules in the disordered region, and that molecular ordering need to provide sufficient overlap of the π-orbitals of conjugated organic molecules to enable efficient charge migration between neighboring molecules.[5–7] Recent advances in the performance of OFETs are largely due to fine control of the morphology and crystalline microstructure in organic semiconductor thin films,[5,6] which can be achieved by tuning the film deposition conditions such as through surface treatment of the substrate,[8,9] modifying solvent properties,[10–12] improving film formation method (spin-casting or drop-casting),[13,14] and the development of new organic semiconductor materials with strong intermolecular π–π interactions.

Acenes are planar organic molecules consisting of *n*-aromatic rings arranged linear and have been intensely investigated over the last decade as promising organic semiconductors because of their low-lying highest occupied molecular orbital (HOMO) energy levels and strong electronic interactions in the solid state.[15] Moreover, control of the intermolecular interactions of acenes can be effectively achieved through molecular design and functionalization. The functionalization of acenes can be used to tune a variety of important properties including their solubility, stability, and intermolecular orientation in crystalline solids. For pentacene, which is now considered a model organic semiconductor, numerous studies of its nucleation and thin-film growth during vapor deposition have been performed; pentacene-based-FETs have been fabricated with field-effect mobilities as high as $3\,cm^2\,V^{-1}\,s^{-1}$.[16–18] Despite its promising electrical properties, pentacene has poor solubility in common organic solvents and edge-to-face herringbone structure that limit efficient charge-carrier transport (Fig. 1a).[19] Bis-triisopropylsilylethynyl pentacene (TIPS_PEN) and bis-triethylsilylethynyl anthradithiophene (TES_ADT) have been synthesized by Anthony and co-workers and found to lack these drawbacks: the substitution of the bulky trialkylsilylethynyl substituent facilitates the close cofacial face-to-face arrangement of the acene backbone (Fig. 1b), and results in dramatic improvements in solubility, stability, and electrical properties.[20–27] Further, small changes in the molecular structure of the substituents in the bulky side groups can lead to significant changes in the intermolecular interactions and the molecular stacking in the

[*] Prof. K. Cho, J. A. Lim, H. S. Lee, W. H. Lee
Department of Chemical Engineering
Pohang University of Science and Technology
Pohang, 790-784 (Korea)
E-mail: kwcho@postech.ac.kr

DOI: 10.1002/adfm.200801135

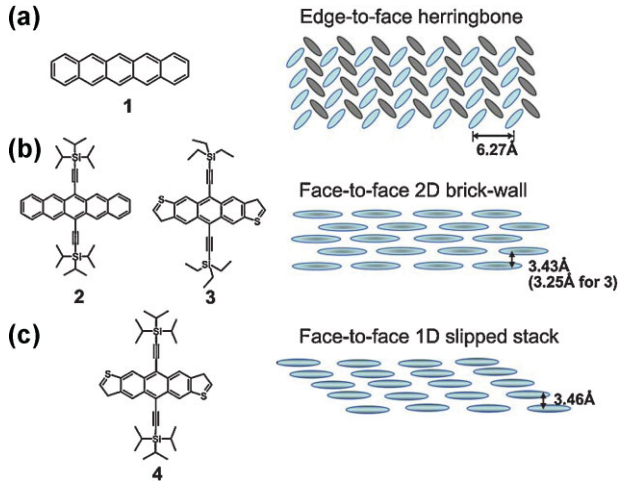

Figure 1. Molecular structures and packing arrangements with average distances between the π-faces in the solid state: **1** pentacene (a), the bis-silylethynylated acene and dithienoathracene derivatives: **2** TIPS_PEN and **3** TES_ADT (b), and **4** triisopropylsilylethynyl anthradithiophene (c).

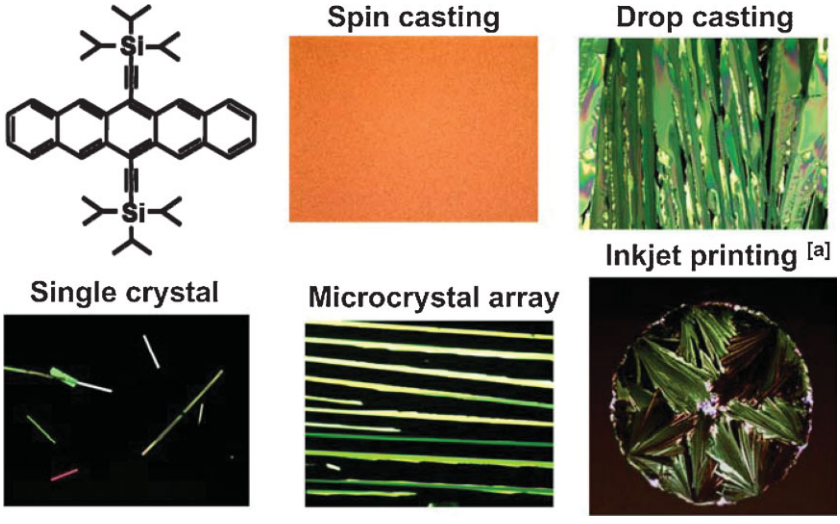

Figure 2. Optical microscopy images of TIPS_PEN thin films with various morphologies and structural developments [a] Reproduced with permission from [35].

solid state, as shown in Figure 1c.[20] In similar approaches, numerous functionalized acenes have been synthesized and their electrical characteristics investigated.[28–33] Comprehensive review articles on functionalized acenes for organic electronic devices are available.[15,34] However, the use of this new class of functionalized acenes in high-performance OFETs requires the development of deposition processes that enable control of the molecular ordering and film morphology.

In this Feature Article, we discuss the strategies for controlling morphology and crystalline microstructure of soluble acenes for use in high-performance OFETs. The resulting film morphologies are dramatically improved for instance from featureless thin films to single crystalline microribbons through this control of the deposition process, even when the same soluble acenes are used, as shown in the optical microscopy (OM) images in Figure 2. We focus on the development of the structures of representative soluble acenes, 6,13-triisopropylsilylethynyl pentacene (TIPS_PEN) and 6,13-triethylsilylethynyl anthradithiophene (TES_ADT), which are the acenes that have been most intensively investigated in recent years because of versatile solution-processability and high charge carrier mobility. The topics discussed in this paper include single crystal and nanowire characteristics, the surface-induced self-organization of thin films, crystallization through annealing and aging, and self-organization in solution-based printing and patterning processes.

2. Single Crystal and Nanowire Characteristics

One of the long-standing challenges in the development of organic FETs is to produce organic single crystals of semiconducting materials.[36–40] Organic single crystals are known not only to have superior device performance[37,41–44] but also to provide a valuable resource for the investigation of the intrinsic parameters that determine charge transport efficiency.[38,45] In particular, the highest mobilities have been found in single crystals of functionalized pentacene because they are largely free of the grain boundaries and molecular disorder that reduce the mobility of the material, and thus the overlapping of the π–π orbitals is enhanced, which promotes efficient charge transport.[46]

TIPS_PEN single crystals have recently been fabricated with the solvent-exchange method in the solution phase by using toluene and acetonitrile as good and poor solvents, respectively.[37] The resulting self-organized single crystals are predominantly straight microribbons with well-defined facets and the following dimensions: height 100–600 nm, width 4–13 μm, and length 40–800 μm, as shown in Figure 3a. The transmission electron microscopy (TEM) image and selective-area electron diffraction (SAED) pattern in Figure 3b show that single crystalline TIPS_PEN forms spontaneously through the facile self-assembly of

Kilwon Cho is a Professor of Chemical Engineering and Director of the Polymer Research Institute at POSTECH in South Korea. He received his B.S. and M. S. in applied chemistry from Seoul National University and his Ph.D. (1986) in polymer science from the University of Akron, and worked as a researcher at IBM Research Center. He has been with POSTECH since 1988. His research interests include polymer thin films, surfaces and interfaces, and organic electronics.

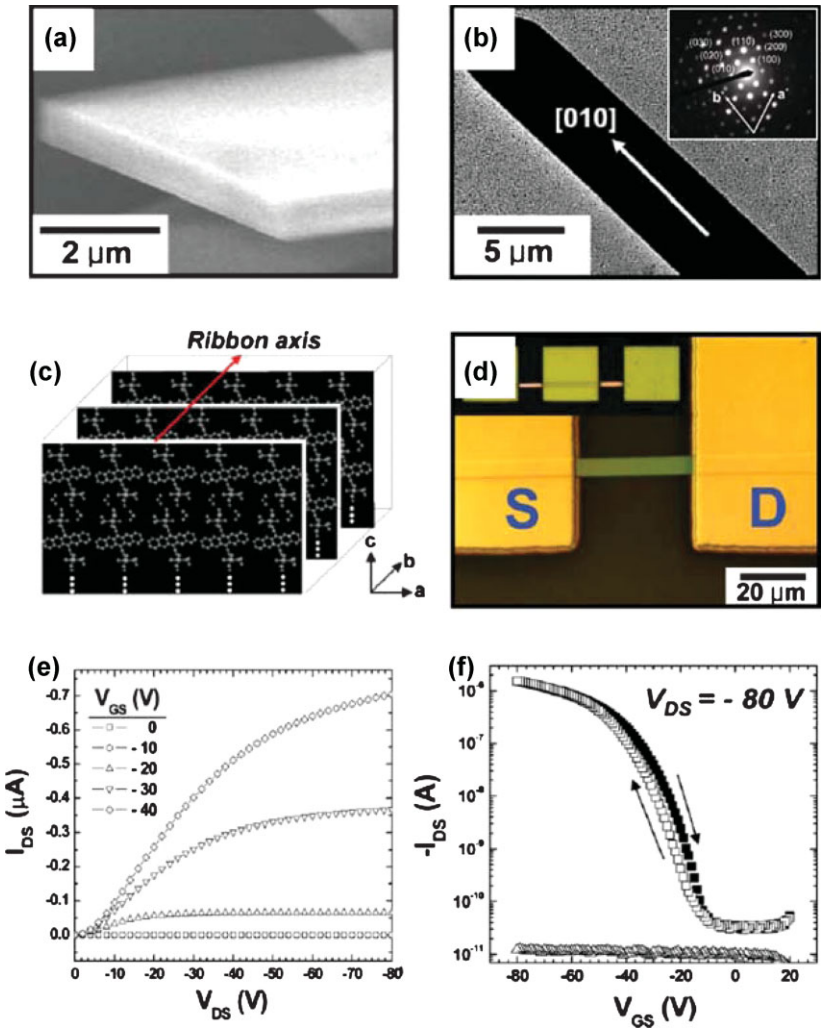

Figure 3. a) SEM image of a TIPS_PEN microribbon on a silicon substrate. b) TEM image of a TIPS_PEN microribbon on a silicon nitride window. The image in the inset shows the SAED pattern of the microribbon. c) Schematic representation of the self-assembly of TIPS_PEN molecules into a single-crystalline microribbon grown along the direction of the π–π stacking. d) OM image of a TIPS_PEN microtransistor. e and f) Typical output and transfer characteristics of OFETs based on individual single crystalline microribbons, respectively. Reproduced with permission from [37].

individual conjugated molecules, which results in preferential well-ordered inter-molecular stacking along the wire/tube axis that coincides with the π–π stacking direction of the TIPS_PEN molecules. A schematic representation of the self-assembly of TIPS_PEN molecules into a single crystalline microribbon is shown in Figure 3c. The field-effect mobility of an FET using 1D single crystalline TIPS_PEN microribbons fabricated on a Si/SiO_2 substrate was found to be 1.42 $cm^2 V^{-1} s^{-1}$, which is one of the highest reported mobilities for an individual 1D organic single crystal fabricated with solution processing.

To understand the intrinsic parameters that determine charge transport efficiency, the anisotropy in soluble acene organic single crystals was studied by using an ultrafast optical pump-terahertz probe technique.[47,48] This technique is useful for the study of the anisotropy of charge carrier mobility in the *a*-*b* plane because it has the advantages of non-contact probing of the charge carrier and transport on subpicosecond time scales.[47–49] The *a*–*b* planes of single crystals of TIPS_PEN (brick-wall-type)[23,50,51] and 6,13-bis(triethylsilylethynyl) pentacene (TES_PEN) (slipped-stack-type)[23] are the largest areas of the crystal surface, with the *a*-axis parallel to the long axis in the TIPS_PEN and TES_PEN crystals shown in Figure 4a and b. To measure the anisotropy of the mobility, each crystal was rotated in the azimuthal (*a*–*b*) plane so that the angle (φ) between the directions of the electric field of the terahertz probe pulse (E_{THz}) and the *a*-axis of the crystal changes. Figure 4c and d show the angular dependence of the charge carrier mobility in the TIPS_PEN and TES_PEN single crystals respectively, normalized to the value at $\varphi = 0^\circ$. According to these results, the ratios of the mobility along the principal axes 1 and 2 of TIPS_PEN and TES_PEN are (3.5 ± 0.6) $(1.04\,\mu_1/0.30\,\mu_2)$ and (12 ± 6) $(1.004\,\mu_1/0.086\,\mu_2)$, respectively (see Fig. 4c and d). The difference between the in-plane mobility anisotropies of TIPS_PEN and TES_PEN single crystals can be explained in terms of crystal structure and molecular packing: 1D charge transport is more favorable in the 1D "slipped-stack-type" structure of the TES_PEN crystals.[51] Thus the mobility anisotropy induced by the degree of π-overlap shows that charges in functionalized pentacene single crystals are mainly transported via a band-like mechanism.[23,38,50–52]

Flexible organic single-crystal nanowires have been fabricated with a simple solution-phase synthesis.[41] Organic nanowires are of importance because of their mechanical flexibility and high electrical performances.[20,28,41,53–56] Figure 5a and b shows the synthesis of hexathiapentacene (HTP), one of the pentacene derivatives, and a dispersion of nanowires in chloroform, respectively. The key to the solution processability of HTP is its insolubility at room temperature, because it can readily be dissolved in and recrystallized from organic solvents with high boiling points such as benzonitrile, nitrobenzene, and *o*-dichlorobenzene; the nanowires are then collected and transferred into a poor solvent such as chloroform. The typical lengths of the nanowires range from several dozen μm to hundreds of μm, with heights in the range 70 to 470 nm. The TEM image and SAED pattern in Figure 5c suggest that in the solution-grown HTP single crystals there is face-to-face molecular stacking along their long axes, which corresponds to the [100] direction or the *a*-axis of the crystal unit cell, with π–π distances of 3.54 Å. HTP single-nanowire FETs exhibit a mobility of 0.27 $cm^2 V^{-1} s^{-1}$, which is six times greater than that of vapor-deposited HTP FETs. The higher mobility of nanowire transistors can be attributed to the high level

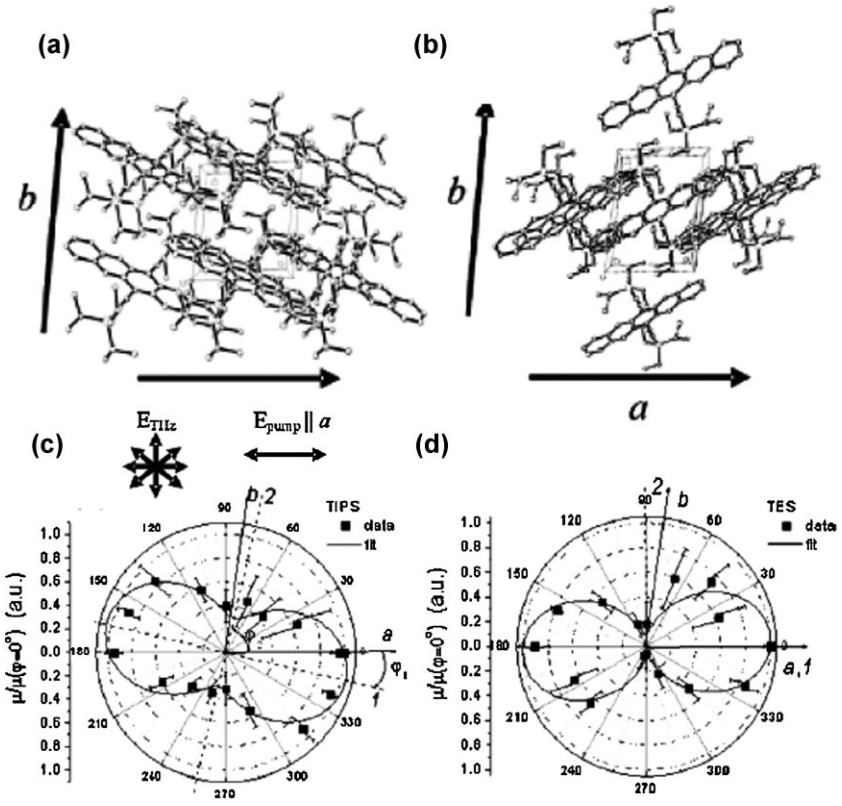

Figure 4. a and b) Molecular packing in TIPS_PEN and TES_PEN crystals, respectively. c and d) Dependence of the charge-carrier mobility in TIPS_PEN and TES_PEN crystals, respectively, on the azimuthal angle (φ). Reproduced with permission from [47]. Copyright 2006 American Institute of Physics.

of structural perfection and the lack of grain boundaries in single-crystal HTP nanowires.[57,58] Furthermore, there is no significant loss in the performance of single-nanowire devices, even after the application of strenuous bending to the flexible substrate because of their flexibility. Further exploration of the mechanical properties of organic single-crystal nanowires has the potential to lead to their use in flexible electronics and displays.

3. Surface-Induced Microstructures

Among the factors affecting field-effect mobility, the molecular ordering of the nanocrystallites in films of organic semiconductors is the most important.[6,8,9,59–61] Attempts to enhance the molecular ordering have focused on the control of the intermolecular interactions at the interface between the layers of device structures.[8,59,61] For examples, the modification of the gate dielectric surface with a self-assembled monolayers (SAMs) can result in differential adsorption or wetting between the channel and field regions of the device, and thus in variation in the surface-induced orientation and device performance.[61–64] The use of SAMs with various functional groups to achieve surface-mediated molecular ordering in polythiophene has been reported, with improvements in field-effect mobilities of more than a factor of 4.[8] In the case of soluble acene, high-performance soluble acene-based transistors have been achieved by using contact-induced crystallization on a SAM-treated electrode.[61] By chemically tailoring the surface properties of electrode contacts, ten of micrometers of crystalline growth can be induced on these contacts into the transistor channel, which significantly impacts the electrical characteristics of the FET device.

Figure 6a and b shows the chemical structures of fluorinated 5,11-bis(triethylsilylethynyl) anthradithiophene (diF-TES_ADT) and pentafluorobenzene thiol (PFBT), which are the organic semiconductor and the electrode treatment material, respectively. The optical microscopy images of the contact and channel regions in Figure 6c and d confirm that the oriented regions with nucleation and growth on top of the contacts extend for more than 10 μm into the channel region. There is a transition in film microstructure in the middle of the transistor channel in device with a greater channel length (L) (Fig. 6c). On the other hand, devices with $L < 20$ μm contain channel regions comprised almost entirely of large grains (Fig. 6d). As a result, the mobility of OFETs with PFBT-treated contacts and $L < 25$ μm is 3–5 times larger because the contact-induced microstructure facilitates charge transport in the channel. In order to explain contact-induced crystallization, it has been suggested that the interaction between the fluorine atoms and sulfur atoms in the thiophene rings on adjacent molecules leads to the rapid formation of a 'tape' motif that precipitates and seeds the growth of the plate-like crystals.[65] The temperature dependence of the current-voltage characteristics for a device is shown as a function of L in Figure 6f, which provides further insight into the relationship between the contact-induced film microstructure and charge transport. As shown in this figure, the mobility is thermally activated between 90 K and 300 K and has a characteristic energy (E_a) that increases with increasing L, from $E_a \approx 0.027$ eV for $L = 10$ μm to $E_a \approx 0.080$ eV for $L = 80$ μm. The large difference between these values of E_a is consistent with the interpretation that the disorder in the channel region decreases with decreasing L, which leads to a reduction in the density of grain boundaries and an increase in the fraction of crystals oriented with the in-plane parallel to the surface due to the crystallization along the chemically tailored contact interfaces.

In general, the surface chemical structure of the dielectric dramatically affects molecular orientation and device performance because the nucleation and growth of molecules on the surface is determined by the balance between the molecules–surface and molecules–molecule interactions.[59,61–64] To study the effects of surface chemical structures on organic semiconducting films, TIPS_PEN films were spin-cast onto substrates with different functionalized (methyl-terminated and phenyl-terminated) SAMs. Figure 7a and b shows the 2D grazing-incidence X-ray diffraction (2D GIXD) patterns of TIPS_PEN films after thermal annealing. Although their surface morphologies are similar, there are significant differences between the

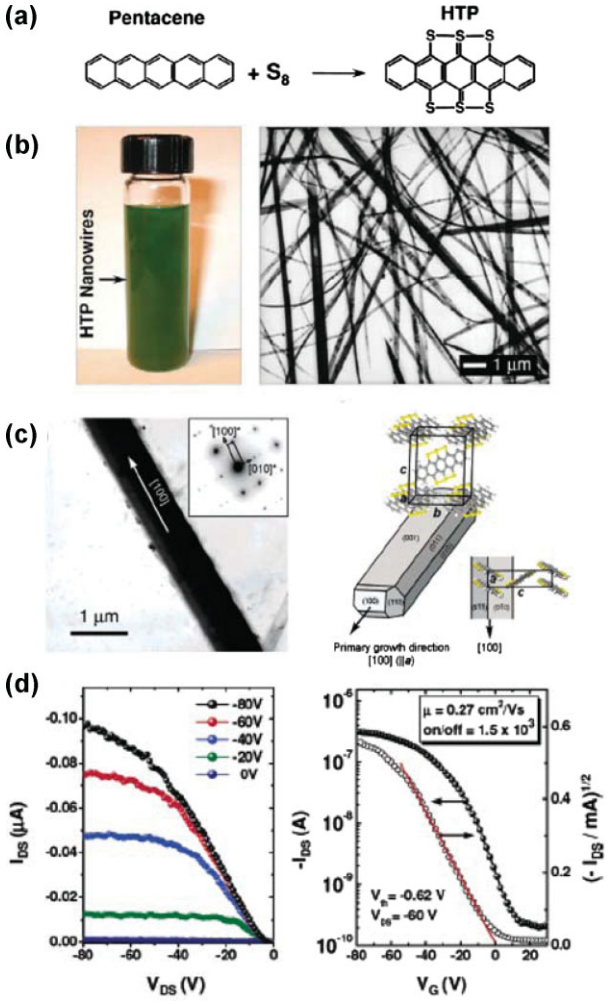

Figure 5. a) The synthesis of HTP. b) Solution dispersion and TEM image of HTP nanowires. c) TEM image of a single-crystal HTP nanowire and growth morphology predicted with the attachment energy method. The inset shows an ED pattern of a single crystal HTP nanowire. d) Output and transfer characteristics of an HTP single nanowire transistor. Reproduced with permission from [41]. Copyright 2007 American Chemical Society.

crystalline natures of these two TIPS_PEN films. The reflection peaks for the q_z and q_{xy} directions for the methyl-terminated substrate consist of highly scattered patterns along the Debye rings. These results mean that the TIPS_PEN films have the imperfect orientation of the TIPS_PEN molecules stacked in a direction perpendicular to the surface for the pentacene ring and there is serious crystal mismatch and dislocation in the vertical and lateral directions.[35] However, for the phenyl-terminated substrate, the scattering of reflection peaks is considerably reduced, and there are many reflection spots in the direction of q_z at a given q_{xy}. These results imply that the crystal perfection and ordering of the TIPS_PEN molecules are enhanced for this SAM, and that well-ordered 3D crystals have formed in the TIPS_PEN film in both the vertical and lateral directions. The improvement in the crystalline nature of the film for the phenyl-terminated case results in enhanced device performance, which is more than 20 times that of the device for the methyl-terminated case. Although the mechanism for the interaction between the phenyl-terminated SAM and the TIPS_PEN molecules is not yet known, different specific interactions between the SAM and the TIPS_PEN molecules might be expected.[66]

4. Crystallization Through Annealing and Aging

The molecular ordering of a spin-cast soluble acene film does not provide optimal π–π interactions between the fused acene rings, so post-deposition treatment such as thermal or solvent-vapor annealing of the film is needed to enhance the molecular ordering of the film while maintaining its uniformity. Thermal annealing is regarded as an effective way to improve the crystallinity of thin films of polymeric semiconductors.[8,67,68] However, clear evidence that thermal annealing enhances the performance of FETs based on soluble acenes has not previously been established because of the complexity of the packing motif and the possible presence of polymorphism in soluble acenes.[23] For example, TIPS_PEN has been reported to exhibit a solid-state phase transition upon heating or cooling.[69] Figure 8a shows a thermal analysis of TIPS_PEN obtained with differential scanning calorimetry (DSC). A characteristic endothermic peak at 124 °C was observed during both Short Cycle and Long Cycle. This peak indicates that TIPS_PEN undergoes a phase transition upon heating. Further, the observed exothermic degradation during the Long Cycle could be interpreted as Diels-Alder polymerization between the alkyne substituent and the pentacene backbone. Cracking of the TIPS_PEN crystals was detected upon heating, as shown in the OM images in Figure 8b, which indicates that thermal expansion and contraction trigger thermally induced strains associated with a change in the packing motif. Figure 8c shows the changes in the packing motif of TIPS_PEN crystals upon thermal annealing. In addition to the changes in the unit cell parameters upon heating, the distances between the acene planes are reduced, which leads to a reduction in the area of overlap of the acene rings. The charge carrier mobility in TIPS_PEN FETs is expected to decrease upon thermal annealing because cracking in the TIPS_PEN crystals leads to a reduction in the number of transport pathways.[69]

Molecular rearrangement of organic semiconductors occurs upon solvent-vapor annealing because the absorbed solvent molecules act as plasticizers on the organic film.[70,71] For this reason, the crystallinity of TES_ADT is increased by a few minutes of solvent-vapor annealing.[72] This rapid change in the molecular ordering probably arises because the soluble acene molecules bind through only weak interactions in the solid state,[51] and thus crystallize readily during solvent-vapor annealing. Figure 9a and c shows the morphologies of spin-cast TES_ADT films before and after dichloroethane-vapor annealing, respectively. This dramatic change in morphology demonstrates that TES_ADT crystals form spontaneously by through π–π interactions between molecules in the presence of solvent. As a result of this change in morphology, the field-effect mobility increases from 0.002 cm^2 V^{-1} s^{-1} (as-prepared FET) to 0.1 cm^2 V^{-1} s^{-1} (FET after dichloroethane-vapor annealing) (Fig. 9b and d). Solvent choice also plays an important role in solvent-vapor annealing. Toluene is a good solvent for TES_ADT,[20] and is also effective in solvent-

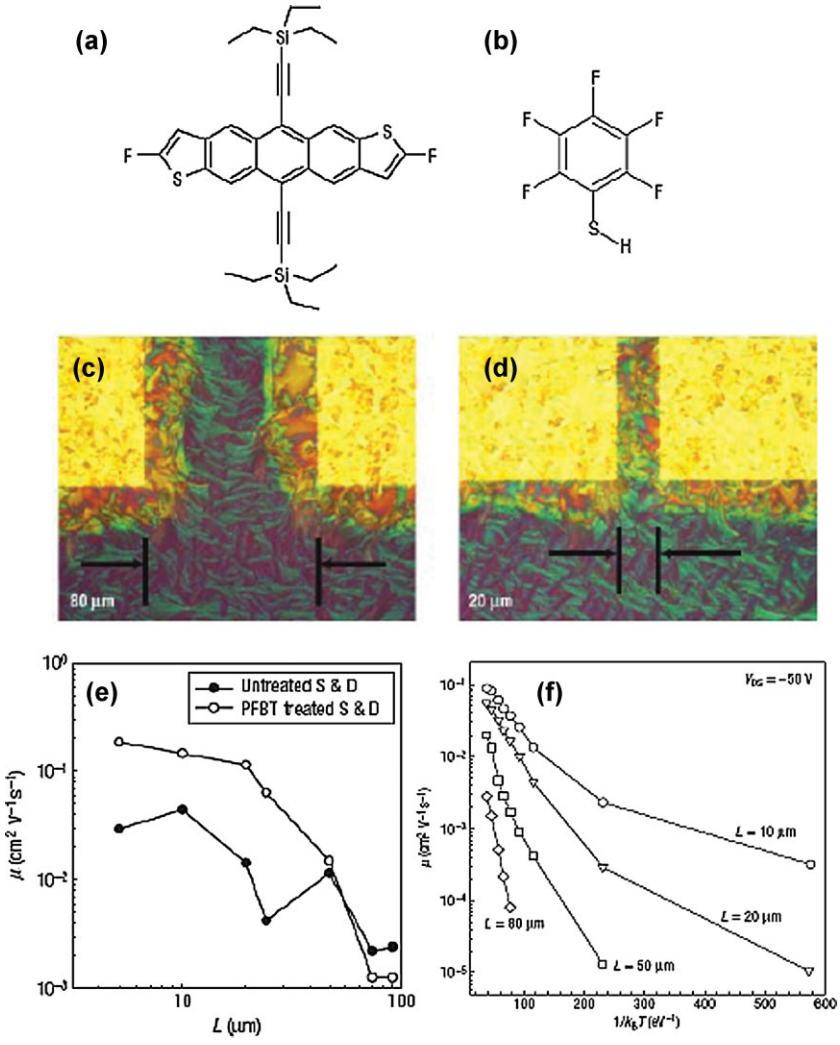

Figure 6. Chemical structures of fluorinated diF-TES_ADT (a) and PFBT (b). Optical micrographs of diF-TESADT TFTs with channel lengths of 80 μm (c) and 20 μm (d). e) Saturation mobility as a function of channel length (*L*) for diF-TESADT FETs with a channel width of 1000 μm and PTBT-treated or untreated contacts. f) Temperature dependence of the effective field-effect mobility in the saturation regime. The devices were fabricated using films spun-cast at 1000 rpm from 2 wt % solutions in room temperature toluene. Reproduced with permission from [61]. Copyright 2008 Nature Publishing Group.

vapor annealing. However, toluene-vapor annealing also induces dewetting of the film, and so results in only a moderate increase in the mobility (0.05 $cm^2 V^{-1} s^{-1}$). Thus, marginal solvents such as dichloroethane are the most effective for solvent-vapor annealing of TES_ADT.[72] X-ray diffraction analysis shows that TES_ADT molecules crystallize with silyl groups on the substrate surface as a result of solvent-vapor annealing (Fig. 9e).[73] Furthermore, the (003) rocking curves in Figure 9f confirm that the lateral coherence lengths of the (*00l*) planes increase sharply upon solvent annealing. Crystals tend to orient so that the surface with low surface energy is parallel to the substrate,[74] and thus in TES_ADT crystals the silyl groups, which have the lowest surface energy, are predominantly oriented along the parallel direction as a result of solvent-vapor annealing. In this way, the π–π interactions between acene backbones are maximized along the in-plane direction, which leads to an increase in the field-effect mobility of TES_ADT-based FETs. The ease with which this material migrates during solvent-vapor annealing also enables the patterning of TES_ADT.[75] UV illumination in the presence of solvent vapors results in the migration of TES_ADT from the substrate surface to a neighboring TES_ADT surface due to the difference between the surface energies of the substrate and TES_ADT. Patterning of TES_ADT with this method can be used to reduce parasitic leakage and the off-currents in FETs.

The weak van der Waals interactions in organic small molecular semiconductors mean that these molecules rearrange even at room temperature.[76,77] Furthermore, since thin films of soluble acenes have low crystallinity immediately after spin-casting, soluble acene molecules can be reorganized by making use of the enthalpic interactions between molecules at room temperature.[78] Figure 10a and b shows the changes in morphology of TES_ADT films as a function of time. The formation and growth of TES_ADT crystallites at room temperature is evident even though no thermal or solvent-vapor annealing has been applied. X-ray diffraction analysis shows that the TES_ADT molecules are tilted with respect to the substrate immediately after spin-casting, but that the number of well-oriented crystals increases with aging time. It has been found that the molecular movement of TES_ADT molecules is sufficiently large to induce conformational changes to stable states in the spin-cast films because TES_ADT has a low glass-transition temperature (close to room temperature). Thus the field-effect mobility of FETs based on these films increased about 100-fold after seven days. These results demonstrate that soluble acenes that exhibit a low crystallinity immediately after spin-casting reorganize into highly crystalline structures when their films are aged at room temperature.[78]

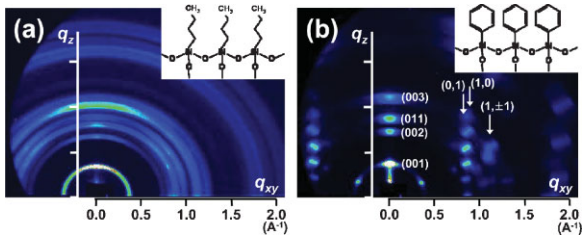

Figure 7. 2D GIXD patterns of thermally annealed TIPS_PEN films after spin-casting onto substrates with methyl-terminated (a) and phenyl-terminated (b) SAMs.

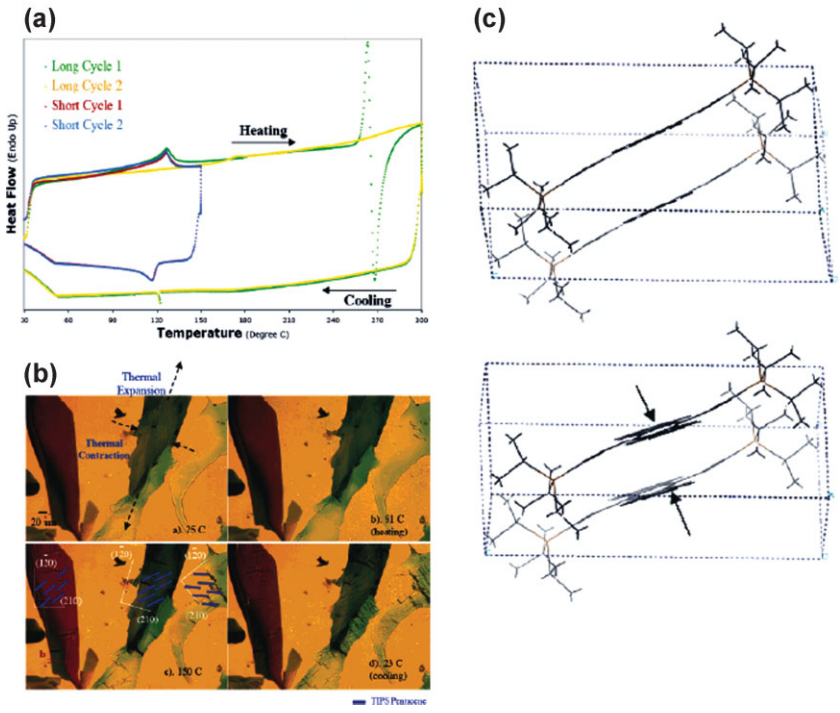

Figure 8. a) Differential scanning calorimetry for TIPS_PEN. Long Cycles 1 and 2 were carried out sequentially on the same sample. b) Hot-stage OM image of TIPS_PEN corresponding to Short Cycle 1 in the DSC. c) Low-temperature (top) and high-temperature TIPS_PEN models (bottom) viewed down the acene plane of the low temperature model. Reproduced with permission from [69]. Copyright 2006 American Chemical Society.

5. Self-Organization of Functionalized Acenes in Printing Processes

There has recently been increased interest in the fabrication of organic transistors with solution-based printing processes such as inkjet and screen printing. The thin-film morphologies and crystalline microstructures of solution-processed organic semiconductors are sensitive to processing conditions, such as the solvent drying rate,[12,24,79] the solubility of molecules,[11,13,80] and the surface properties of the substrate.[8] In particular, the drying behavior during solution processing has a critical role in the self-organization of organic semiconductor molecules. The recently reported drying-mediated self-assembly of nanoparticles,[81] diblock copolymers,[82] and carbon nanotubes[83] indicates that control of the evaporation-induced flows of solvent during a drying process is important to the self-assembly of organic semiconductor molecules during solution processing because solvent flows can easily transport the molecules.

The fabrication of one-dimensional crystal arrays of TIPS_PEN has been accomplished by controlling the evaporation behavior of the solvent during simple drop casting on a tilted substrate (Fig. 11a and b).[84] The substrate is tilted so that the lower drop line spreads down the slide and the upper contact line remains pinned. When the contact line of a solution drop is pinned in a drying process, the evaporation near the upper contact line is faster than near the lower drop line, which results in a hydrodynamic flow of the solvent toward the upper contact line to compensate for evaporation loss and thus in the transport of the TIPS_PEN molecules to the contact line.[85] Hence the crystal seeds nucleation from the pinned contact line, and crystallites oriented with the stacking axis grow down the slide (Fig. 11c). X-ray diffraction patterns of such 1D crystal arrays have confirmed that the TIPS_PEN molecules are preferentially stacked along the (100) axis in the direction of the crystal growth, as shown in Figure 11d. This 2D brick-wall stacking arrangement of TIPS_PEN maximizes the π-overlap along the *a*-axis, which implies that directional crystal growth along the (100) axis between the source and drain electrodes is optimal for use in FETs. A FET device based on directionally-aligned crystals was found to exhibit a high field-effect mobility of 0.3 cm^2 V^{-1} s^{-1} and an on/off current ratio of 10^6.

Inkjet printing has received special attention as a patterning technique for the cost-effective fabrication of organic electronics.[85,86] The morphology and crystalline microstructure of inkjet-printed TIPS_PEN thin films are strongly dependent on their drying behavior. One approach to control of the hydrodynamic flows in a drying droplet is the use of a mixed-solvent system,[35,87–89] In general, there are two types of evaporation-induced flows: convective flow toward the contact line from the interior of the droplet, and Marangoni flow, which is induced by the surface tension gradient between regions with low and regions with high surface tension.[90] The outward convective flow can be enhanced or counterbalanced by Marangoni flow, depending on the solvent composition. A ring-like deposit that marks the perimeter of the droplet results from the inkjet printing of a TIPS_PEN single dot from chlorobenzene (b.p. 131 °C) homo-solvent, as shown in Figure 12a and e.[35] This ring stain is induced by convective flow and is explained by the "coffee-stain" effect demonstrated by Deegan and co-workers.[91] The crystalline microstructure was investigated with GI-XRD and it was found that the printed TIPS_PEN film with this uneven ring morphology has a randomly oriented nanocrystalline structure, which has inferior charge carrier transport properties in an FET device. In contrast, a uniform morphology was found to result from the use of dichlorobenzene, which has a high boiling point (180 °C), as a minor solvent; the presence of dichlorobenzene might reduce the convective flow by slowing evaporation at the contact edge (Fig. 12c and g). However, it was found that this uniform morphology does not guarantee a well-ordered crystalline structure. More interestingly, self-aligned crystals with three-dimensional well-ordered crystalline structure are obtained when recirculation flow is generated in the drying droplet by Marangoni flow in the opposite direction to the convective flow, which is induced by using dodecane as a minor solvent; dodecane has a higher boiling point (216 °C) and a lower surface tension (25.3 dyn cm^{-1}) than the main solvent (chlorobenzene) (Fig. 12d). Nucleation occurs at the contact line of the droplet and the crystal

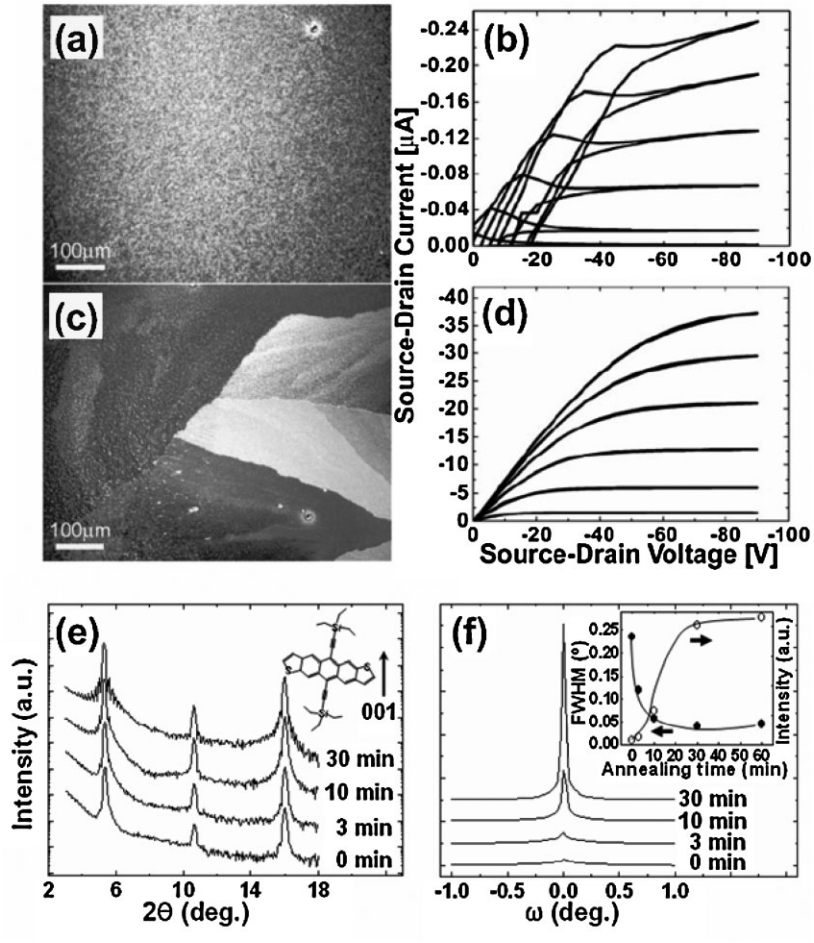

Figure 9. a) An optical microscopy image and b) the corresponding output characteristics of an as-spun TES_ADT FET ($W/L = 9.5$). c) An optical microscopy image and d) the corresponding output characteristics of a dichloroethane-vapor annealed FET. Reproduced with permission from [72]. e) X-ray diffraction patterns of TES_ADT films for various solvent-annealing times. The inset shows a TES_ADT molecule with molecular orientation along the (001) axis. f) Rocking curves on the (003) reflections for various annealing times. The inset shows the changes in the full width half maximum (FWHM) in the rocking scans and in the intensity of the (003) reflections with annealing time (min). Reproduced with permission from [73]. Copyright 2007 American Institute of Physics.

growth proceeds from the edge to the center of the droplet. These self-aligned TIPS_PEN crystals were used to fabricate high-performance field-effect transistors with an effective field-effect mobility of $0.12\,cm^2\ V^{-1}\ s^{-1}$, which demonstrates that optimization of the solvent composition can be used to control the morphology and molecular ordering of inkjet-printed soluble acene thin films.

An alternative approach to the control of the drying behavior of droplets is to vary the surface energy of the substrate.[92] In particular, because the surface energy and chemical composition of the dielectrics in organic transistors significantly influence device performance,[8,93,94] it is important to understand how dielectric surface wettability determines the morphology and crystalline microstructure of inkjet-printed organic semiconductors. In fact, the different drying behaviors of droplets on surface-modified SiO_2 dielectrics with different SAMs result in inkjet-printed TIPS_PEN films with significantly different morphologies and crystalline microstructures as shown in Figure 13. On a hydrophilic surface with a high surface energy, TIPS_PEN microcrystals with highly ordered crystalline structure develop from the periphery to the interior of the droplet (Fig. 13a), which is attributed to contact line pinning and outward convective flow in the drying droplet. In contrast, small agglomerates with poor molecular ordering form on a hydrophobic surface with a low surface energy (Fig. 13b), because continuous retraction of the contact line occurs during drying process in the absence of pinning of contact line. However, the nature of contact lines during evaporation and drying-mediated self-organization in a drying solution are complex phenomena that depend on energy dissipation, molecular diffusion, and the molecular interactions between the solvent, the solute, and the substrate. Further investigation of the effects of evaporation behavior on the drying-mediated self-organization of soluble acenes is required.

In addition, directionally crystallized TIPS_PEN thin films have been fabricated with a direct write method that uses a pen.[95] Film deposition is achieved by allowing a microdroplet of solution on the end of the pen to make contact with the surface of substrate and then laterally translating the pen at a controlled rate, and as a result the crystalline grains extend from the edge of the line inward at an angle inclined toward the writing direction. Such aligned crystals have been used in studies of the correlation between grain structure and charge-carrier transport.

6. Conclusion

Although the development of organic semiconductors has the potential to enable inexpensive electronic device fabrication, high-performance FETs with solution-deposited semiconducting films have not yet been achieved. In pursuit of this goal, an ever-expanding number of functionalized acenes have been synthesized as organic semiconductors, with the aim of controlling their intermolecular interactions and thus achieving desirable molecular packing in their crystalline microstructures. In this article, we have discussed the ways in which precise control of the film formation process can be used to optimize molecular orientation and structural development, and thus to enhance charge carrier transport properties. Fine control of the solubility of soluble acene molecules, the molecular interactions at the substrate interface, and the drying conditions in solution-based film-deposition processes can be used to tailor the morphologies and crystalline microstructures of organic semiconductors, ranging from single crystals to directionally aligned crystal arrays. Further, self-organization in solid-state films can be

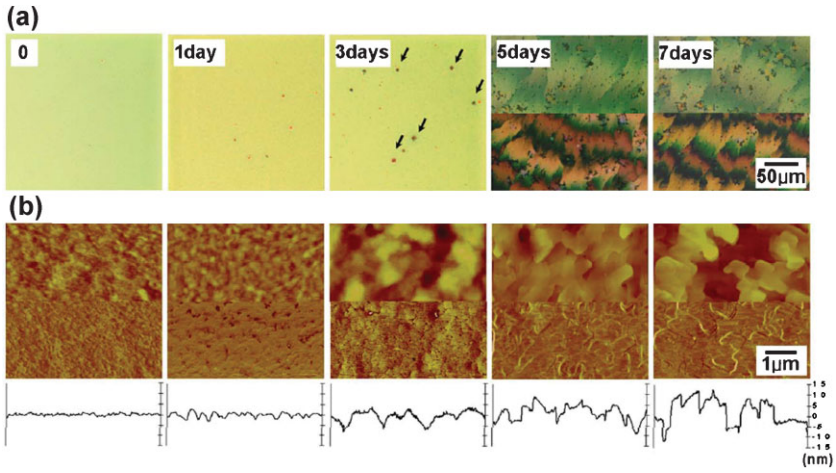

Figure 10. a) Optical microscopy images and b) atomic force microscopy images (top: topographical, middle: phase, and bottom: height profiles) of TES_ADT films for various aging times (0, 1, 3, 5, and 7 days). Additional OM images were collected on days 5 and 7 by using a polarizing angle of 90° (see images, lower half). Reproduced with permission from [78].

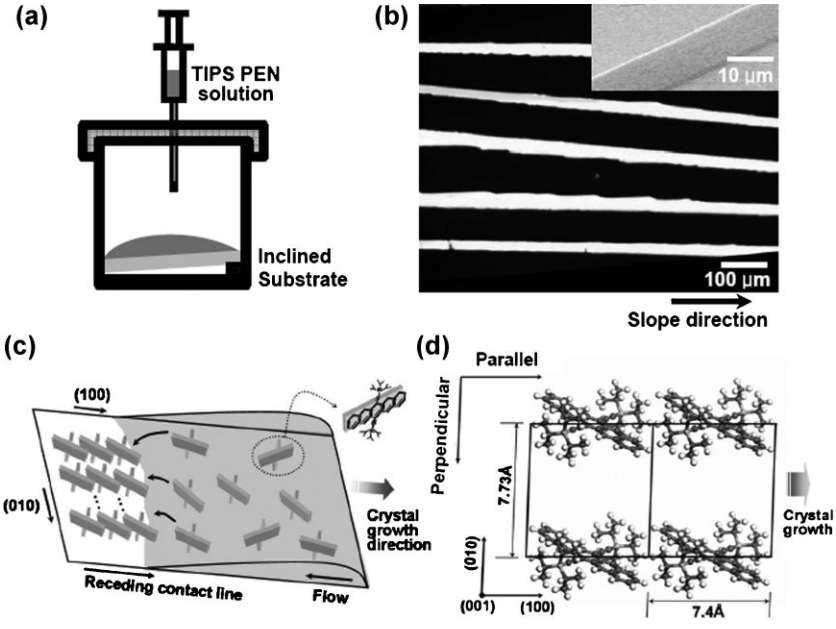

Figure 11. a) Schematic diagram of the fabrication process. b) Polarized optical microscopy image of an array of ribbon-shaped TIPS_PEN crystals directed down a slide (inset: FE-SEM image of a TIPS_PEN crystal with a well-defined edge). c) Possible growth mechanism for TIPS_PEN crystal arrays with a stacking (100) axis. d) In-plane stacking geometry for parallel and perpendicular incident beam directions. Reproduced with permission from [84]. Copyright 2007 American Institute of Physics.

induced by using thermal or solvent-vapor annealing or aging. Based on these results, we expect that further efforts in the development of organic semiconductors, and of special techniques such as discussed above for the control of morphology and molecular ordering, will result in significant breakthroughs in organic electronics.

Acknowledgements

This work was supported by a grant (F0004021-2008-31) from the Information Display R&D Center under the 21st Century Frontier R&D Program, Creative Research Initiative-Acceleration Research (R17-2008-029-01000-0), the ERC Program of KOSEF (R11-2003-006-06004-0), a grant (RTI 04-01-04) from the Regional Technology Innovation Program, and the POSTECH Core Research Program. The authors thank the Pohang Accelerator Laboratory for providing the synchrotron radiation sources at 4C2, 8C1, and 10C1 beam lines used in this study. This article is part of a special issue on Materials Science in Korea.

Received: August 3, 2008
Published online: December 30, 2008

[1] H. Sirringhaus, T. Kawase, R. H. Friend, T. Shimoda, M. Inbasekaran, W. Wu, E. P. Woo, *Science* **2000**, *290*, 2123.
[2] G. Horowitz, *J. Mater. Res.* **2004**, *19*, 1946.
[3] S. R. Forrest, *Nature* **2004**, *428*, 911.
[4] W. Clemens, W. Fix, J. Ficker, A. Knobloch, A. Ullmann, *J. Mater. Res.* **2004**, *19*, 1963.
[5] M. M. Ling, Z. Bao, *Chem. Mater.* **2004**, *16*, 4824.
[6] Y. D. Park, J. A. Lim, H. S. Lee, K. Cho, *Mater. Today* **2007**, *10*, 46.
[7] H. Sirringhaus, *Adv. Mater.* **2005**, *17*, 2411.
[8] D. H. Kim, Y. D. Park, Y. Jang, H. Yang, Y. H. Kim, J. I. Han, D. G. Moon, S. Park, T. Chang, C. Chang, M. Joo, C. Y. Ryu, K. Cho, *Adv. Funct. Mater.* **2005**, *15*, 77.
[9] H. Yang, T. J. Shin, M.-M. Ling, K. Cho, C. Y. Ryu, Z. Bao, *J. Am. Chem. Soc.* **2005**, *127*, 11542.
[10] J.-F. Chang, B. Sun, D. W. Breiby, M. M. Nielsen, T. I. Solling, M. Giles, I. McCulloch, H. Sirringhaus, *Chem. Mater.* **2004**, *16*, 4772.
[11] H. Yang, T. J. Shin, L. Yang, K. Cho, C. Y. Ryu, Z. Bao, *Adv. Funct. Mater.* **2005**, *15*, 671.
[12] Y.-H. Kim, Y. U. Lee, J.-I. Han, S.-M. Han, M.-K. Han, *J. Electrochem. Soc.* **2007**, *154*, H995.
[13] H. Yang, S. W. LeFevre, C. Y. Ryu, Z. Bao, *Appl. Phys. Lett.* **2007**, *90*, 172116.
[14] D. M. DeLongchamp, B. M. Vogel, Y. Jung, M. C. Gurau, C. A. Richter, O. A. Kirillov, J. Obrzut, D. A. Fischer, S. Sambasivan, L. J. Richter, E. K. Lin, *Chem. Mater.* **2005**, *17*, 5610.
[15] J. E. Anthony, *Angew. Chem. Int. Ed.* **2008**, *47*, 452.
[16] R. Ruiz, D. Choudhary, B. Nickel, T. Toccoli, K.-C. Chang, A. C. Mayer, P. Clancy, J. M. Blakely, R. L. Headrick, S. Iannotta, G. G. Malliaras, *Chem. Mater.* **2004**, *16*, 4497.
[17] H. S. Lee, D. H. Kim, J. H. Cho, Y. D. Park, J. S. Kim, K. Cho, *Adv. Funct. Mater.* **2006**, *16*, 1859.
[18] T. W. Kelley, D. V. Muyres, P. F. Baude, T. P. Smith, T. D. Jones, *Mater. Res. Soc. Symp. Proc.* **2003**, *771*, L6.5.1.
[19] R. B. Campbell, J. M. Robertson, J. Trotter, *Acta Crystallogr.* **1961**, *14*, 705.
[20] M. M. Payne, S. R. Parkin, J. E. Anthony, C.-C. Kuo, T. N. Jackson, *J. Am. Chem. Soc.* **2005**, *127*, 4986.
[21] J. E. Anthony, J. S. Brooks, D. L. Eaton, S. R. Parkin, *J. Am. Chem. Soc.* **2001**, *123*, 9482.

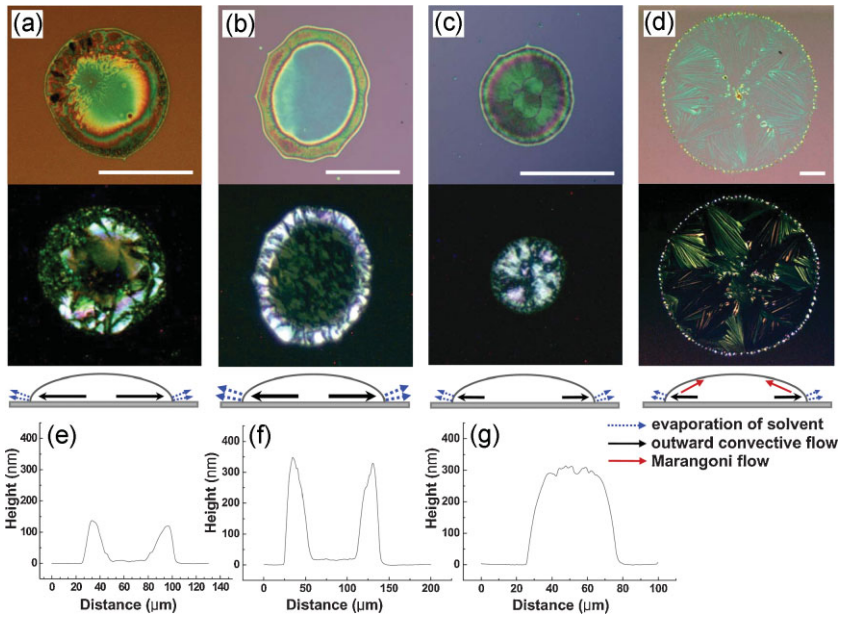

Figure 12. Optical microscopy and polarized images of inkjet-printed TIPS_PEN droplets with various solvent compositions: a) chlorobenzene and mixed-solvents containing chlorobenzene and 25 vol % b) hexane, c) *o*-dichlorobenzene, and d) dodecane. Schematic diagrams of the evaporation-induced flow in a droplet during drying are shown for various solvent compositions under the OM images. The height profiles of the TIPS_PEN single dots printed from e) chlorobenzene and solvent mixtures with f) hexane and g) o-dichlorobenzene are shown at the bottom (scale bar = 50 μm). Reproduced with permission from [35].

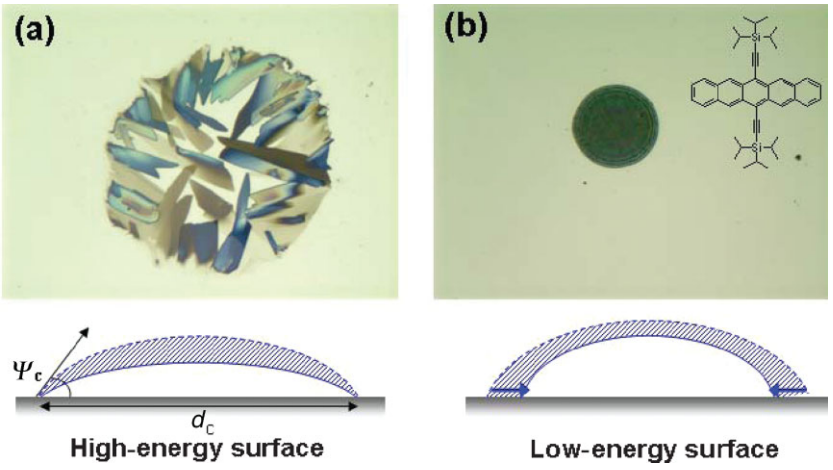

Figure 13. Optical microscopy images and schematic illustrations of the drying behavior of inkjet-printed TIPS_PEN single droplets deposited on a) a high-energy surface and b) a low-energy surface.

[22] C. D. Sheraw, T. N. Jackson, D. L. Eaton, J. E. Anthony, *Adv. Mater.* **2003**, *15*, 2009.
[23] J. E. Anthony, D. L. Eaton, S. R. Parkin, *Org. Lett.* **2002**, *4*, 15.
[24] S. K. Park, T. N. Jackson, J. E. Anthony, D. A. Mourey, *Appl. Phys. Lett.* **2007**, *91*, 063514.
[25] J. G. Park, R. Vasic, J. S. Brooks, J. E. Anthony, *J. Appl. Phys.* **2006**, *100*, 044511.
[26] J.-P. Hong, A.-Y. Park, S. Lee, J. Kang, N. Shin, D. Y. Yoon, *Appl. Phys. Lett.* **2008**, *92*, 143311.
[27] K. C. Dickey, T. J. Smith, K. J. Stevenson, S. Subramanian, J. E. Anthony, Y.-L. Loo, *Chem. Mater.* **2007**, *19*, 5210.
[28] K. Kobayashi, R. Shimaoka, M. Kawahata, M. Yamanaka, K. Yamaguchi, *Org. Lett.* **2006**, *8*, 2385.
[29] J. E. Anthony, J. Gierschner, C. A. Landis, S. R. Parkin, J. B. Shermana, R. C. Bakus, *Chem. Commun.* **2007**, 4746.
[30] Q. Miao, X. Chi, S. Xiao, R. Zeis, M. Lefenfeld, T. Siegrist, M. L. Steigerwald, C. Nuckolls, *J. Am. Chem. Soc.* **2006**, *128*, 1340.
[31] T. Okamoto, Z. Bao, *J. Am. Chem. Soc.* **2007**, *129*, 10308.
[32] J. Chen, S. Subramanian, S. R. Parkin, M. Siegler, K. Gallup, C. Haughn, D. C. Martin, J. E. Anthony, *J. Mater. Chem.* **2008**, *18*, 1961.
[33] R. Schmidt, S. Gőttling, D. Leusser, D. Stalke, A.-M. Krause, F. Würthner, *J. Mater. Chem.* **2006**, *16*, 3708.
[34] J. E. Anthony, *Chem. Rev.* **2006**, *106*, 5028.
[35] J. A. Lim, W. H. Lee, H. S. Lee, J. H. Lee, Y. D. Park, K. Cho, *Adv. Funct. Mater.* **2008**, *18*, 229.
[36] E. W. Meijer, A. P. H. J. Schenning, *Nature* **2002**, *419*, 353.
[37] D. H. Kim, D. Y. Lee, H. S. Lee, W. H. Lee, Y. H. Kim, J. I. Han, K. Cho, *Adv. Mater.* **2007**, *19*, 678.
[38] V. Podzorov, E. Menard, A. Borissov, V. Kiryukhin, J. A. Rogers, M. E. Gershenson, *Phys. Rev. Lett.* **2004**, *93*, 866021.
[39] S. C. B. Mannsfeld, A. L. Briseno, S. Liu, C. Reese, M. E. Roberts, Z. Bao, *Adv. Funct. Mater.* **2007**, *17*, 3545.
[40] C. D. Dimitrakopoulos, P. R. L. Malenfant, *Adv. Mater.* **2002**, *14*, 99.
[41] A. L. Briseno, S. C. B. Mannsfeld, X. Lu, Y. Xiong, S. A. Jenekhe, Z. Bao, Y. Xia, *Nano Lett.* **2007**, *7*, 668.
[42] V. C. Sundar, J. Zaumseil, V. Podzorov, E. Menard, R. L. Willett, T. Someya, M. E. Gershenson, J. A. Rogers, *Science* **2004**, *303*, 1644.
[43] D. H. Kim, J. T. Han, Y. D. Park, Y. Jang, J. H. Cho, M. Hwang, K. Cho, *Adv. Mater.* **2006**, *18*, 719.
[44] C. Reese, Z. Bao, *Mater. Today* **2007**, *10*, 20.
[45] J. Y. Lee, S. Roth, Y. W. Park, *Appl. Phys. Lett.* **2006**, *88*, 252106.
[46] V. Podzorov, S. E. Sysoev, E. Loginova, V. M. Pudalov, M. E. Gershenson, *Appl. Phys. Lett.* **2003**, *83*, 3504.
[47] O. Ostroverkhova, D. G. Cooke, F. A. Hegmann, R. R. Tykwinski, S. R. Parkin, J. E. Anthony, *Appl. Phys. Lett.* **2006**, *89*, 192113.
[48] F. A. Hegmann, R. R. Tykwinski, K. P. H. Lui, J. E. Bullock, J. E. Anthony, *Phys. Rev. Lett.* **2002**, *89*, 227403.
[49] C. A. Schmuttenmaer, *Chem. Rev.* **2004**, *104*, 1759.
[50] R. C. Haddon, X. Chi, M. E. Itkis, J. E. Anthony, D. L. Eaton, T. Siegrist, C. C. Mattheus, T. T. M. Palstra, *J. Phys. Chem. B* **2002**, *106*, 8288.
[51] A. Troisi, G. Orlandi, J. E. Anthony, *Chem. Mater.* **2005**, *17*, 5024.
[52] O. Ostroverkhova, D. G. Cooke, S. Shcherbyna, R. F. Egerton, F. A. Hegmann, R. R. Tykwinski, J. E. Anthony, *Phys. Rev. B* **2005**, *71*, 035204.
[53] A. L. Briseno, S. C. B. Mannsfeld, S. A. Jenekhe, Z. Bao, Y. Xia, *Mater. Today* **2008**, *11*, 38.
[54] Q. X. Tang, H. X. Li, M. He, W. P. Hu, C. Liu, K. Chen, C. Wang, Y. Q. Liu, D. B. Zhu, *Adv. Mater.* **2006**, *18*, 65.

[55] S. X. Xiao, J. Y. Tang, T. Beetz, X. F. Guo, N. Tremblay, T. Siegrist, Y. M. Zhu, M. Steigerwald, C. Nckolls, *J. Am. Chem. Soc.* **2006**, *128*, 10700.
[56] H. Meng, M. Bendikov, G. Mitchell, R. Helgeson, F. Wudl, Z. Bao, T. Siegrest, Ch. Kloc, C.-H. Chen, *Adv. Mater.* **2003**, *15*, 1090.
[57] M. E. Gershenson, V. Podzorov, A. F. Morpurgo, *Rev. Mod. Phys.* **2006**, *78*, 973.
[58] A. L. Briseno, R. J. Tseng, M.-M. Ling, E. H. L. Falcao, Y. Yang, F. Wudl, Z. Bao, *Adv. Mater.* **2006**, *18*, 2320.
[59] D. H. Kim, H. S. Lee, H. Yang, L. Yang, K. Cho, *Adv. Funct. Mater.* **2008**, *18*, 1363.
[60] Y. D. Park, D. H. Kim, Y. Jang, J. H. Cho, M. Hwang, H. S. Lee, J. A. Lim, K. Cho, *Org. Electron.* **2006**, *7*, 514.
[61] D. J. Gundlach, J. E. Royer, S. K. Pak, S. Subramanian, O. D. Jurchescu, B. H. Hamadani, A. J. Moad, R. J. Kline, L. C. Teague, O. Kirillov, C. A. Richter, J. G. Kushmerick, L. J. Richter, S. R. Parkin, T. N. Jackson, J. E. Anthoney, *Nat. Mater.* **2008**, *7*, 216.
[62] H. Y. Choi, S. H. Kim, J. Jang, *Adv. Mater.* **2004**, *16*, 732.
[63] S. Steudel, D. Janssen, S. Verlaak, J. Genoe, P. Heremans, *Appl. Phys. Lett.* **2004**, *85*, 5550.
[64] A. L. Briseno, S. C. B. Mannsfeld, M. M. Ling, S. Liu, R. J. Tseng, C. Reese, M. E. Roberts, Y. Yang, F. Wudl, Z. Bao, *Nature* **2006**, *444*, 913.
[65] K. Reichenbächer, H. I. Süss, J. Hulliger, *Chem. Soc. Rev.* **2005**, *34*, 22.
[66] A. L. Briseno, J. Aizenberg, Y.-J. Han, R. A. Penkala, H. Moon, A. J. Lovinger, C. Kloc, Z. Bao, *J. Am. Chem. Soc.* **2005**, *127*, 12164.
[67] B. S. Ong, Y. Wu, P. Liu, S. Gardner, *J. Am. Chem. Soc.* **2004**, *11*, 3378.
[68] R. J. Kline, M. D. Mcgehee, M. F. Toney, *Nat. Mater.* **2006**, *5*, 222.
[69] J. Chen, J. Anthony, D. C. Martin, *J. Phys. Chem. B* **2006**, *110*, 16397.
[70] Y. Lin, M. Müller, K. Binder, *J. Chem. Phys.* **2004**, *121*, 3816.
[71] D. J. Mascaro, M. E. Thompson, H. I. Smith, V. Bulovic, *Org. Electron.* **2005**, *6*, 211.
[72] K. C. Dickey, J. E. Anthony, Y.-L. Loo, *Adv. Mater.* **2006**, *18*, 1721.
[73] W. H. Lee, D. H. Kim, J. H. Cho, Y. Jang, J. A. Lim, D. Kwak, K. Cho, *Appl. Phys. Lett.* **2007**, *91*, 092105.
[74] J. E. Northrup, *Phys. Rev. B* **2002**, *66*, 121404.
[75] K. C. Dickey, S. Subramanian, J. E. Anthony, L.-H. Han, S. Chen, Y.-L. Loo, *Appl. Phys. Lett.* **2007**, *90*, 244103.
[76] E.-M. Han, L.-M. Do, M. Fujihira, H. Inada, Y. Shirota, *J. Appl. Phys.* **1996**, *80*, 3297.
[77] W. L. Kalb, F. Meier, K. Mattenberger, B. Batlogg, *Phys. Rev. B* **2007**, *76*, 184112.
[78] W. H. Lee, J. A. Lim, D. H. Kim, J. H. Cho, Y. Jang, Y. H. Kim, J. I. Han, K. Cho, *Adv. Funct. Mater.* **2008**, *18*, 560.
[79] D. H. Kim, Y. D. Park, Y. Jang, K. Cho, *Macromol. Rapid Commun.* **2005**, *26*, 834.
[80] N. Kiriy, E. Jähne, H.-J. Adler, M. Schneider, A. Kiriy, G. Gorodyska, S. Minko, D. Jehnichen, P. Simon, A. A. Fokin, M. Stamm, *Nano Lett.* **2003**, *3*, 707.
[81] T. P. Bigoni, X.-M. Lin, T. T. Nguyen, E. I. Corwin, T. A. Witten, H. M. Jaeger, *Nat. Mater.* **2006**, *5*, 265.
[82] M. Kimura, M. J. Misner, T. Xu, S. H. Kim, T. P. Russell, *Langmuir* **2003**, *19*, 9910.
[83] R. Duggal, F. Hussain, Pasquali, *Adv. Mater.* **2006**, *18*, 29.
[84] W. H. Lee, D. H. Lim, Y. Jang, J. H. Cho, Y. H. Kim, J. I. Han, K. Cho, *Appl. Phys. Lett.* **2007**, *90*, 132106.
[85] B. J. de Gans, P. C. Duineveld, U. S. Schubert, *Adv. Mater.* **2004**, *16*, 203.
[86] R. A. Street, W. S. Wong, S. E. Ready, M. L. Chabinyc, A. C. Arias, S. Limb, A. Salleo, R. Lujan, *Mater. Today* **2006**, *9*, 32.
[87] B. J. de Gans, U. S. Schubert, *Langmuir* **2004**, *20*, 7789.
[88] J. Park, J. Moon, *Langmuir* **2006**, *22*, 3506.
[89] J. A. Lim, J. H. Cho, Y. D. Park, D. H. Kim, M. Hwang, K. Cho, *Appl. Phys. Lett.* **2006**, *88*, 082102.
[90] D. Pesach, A. Marmur, *Langmuir* **1987**, *3*, 519.
[91] R. D. Deegan, O. Bakajin, T. F. Dupont, G. Huber, S. R. Nagel, T. A. Witten, *Nature* **1997**, *389*, 827.
[92] K. Uno, K. Hayashi, T. Hayashi, K. Ito, H. Kitano, *Colloid Polym. Sci.* **1998**, *276*, 810.
[93] S. Kobayashi, T. Nishikawa, T. Takenobu, S. Mori, T. Shimoda, T. Mitani, H. Shimotani, N. Yoshimoto, S. Ogawa, Y. Iwasa, *Nat. Mater.* **2004**, *3*, 317.
[94] Y. Jang, J. H. Cho, D. H. Kim, Y. D. Park, M. Hwang, K. Cho, *Appl. Phys. Lett.* **2007**, *90*, 132104.
[95] R. L. Headrick, S. Wo, F. Sansoz, J. E. Anthony, *Appl. Phys. Lett.* **2008**, *92*, 063302.